

# Neutron stars in the bumblebee theory of gravity

Peixiang Ji,<sup>1,2</sup> Zhuhai Li,<sup>1,2</sup> Lirui Yang,<sup>3</sup> Rui Xu,<sup>4</sup> Zexin Hu,<sup>1,2</sup> and Lijing Shao<sup>2,5,\*</sup>

<sup>1</sup>*Department of Astronomy, School of Physics, Peking University, Beijing 100871, China*

<sup>2</sup>*Kavli Institute for Astronomy and Astrophysics, Peking University, Beijing 100871, China*

<sup>3</sup>*Cavendish Laboratory, JJ Thompson Avenue, Cambridge CB3 0HE, UK*

<sup>4</sup>*Department of Astronomy, Tsinghua University, Beijing 100084, China*

<sup>5</sup>*National Astronomical Observatories, Chinese Academy of Sciences, Beijing 100012, China*

Recently, theoretical studies on the bumblebee gravity model, a nonminimally-coupled vector-tensor theory that violates the Lorentz symmetry, have flourished, with a simultaneous increase in the utilization of observations to impose constraints. The static spherical solutions of neutron stars (NSs) in the bumblebee theory are calculated comprehensively in this work. These solutions with different coupling constants reveal a rich theoretical landscape for NSs, including vectorized NSs and NSs with finite radii but divergent masses. With these solutions, preliminary constraints on the asymptotic vector field values are obtained through restrictions on the stellar radius.

## I. INTRODUCTION

Compact stars, generating extremely strong gravitational field, are among the few environments where strong-field tests of gravity can be conducted [1–8]. Merging compact star binaries that emit strong gravitational waves (GWs) have enhanced our understanding of dense matter and strong-field gravity [1, 9, 10]. The study of gravitational astrophysics has entered a more precise multi-messenger era, following the observations of GW170817 and GRB170817A [11–14]. Studying neutron stars (NSs) in modified gravity theories has a long history. In early studies of NSs in scalar-tensor theories [15], it was found that a NS could acquire a scalar charge, leading to nonperturbative effects within the star. These energetically favored scalarized NSs can spontaneously transform from their corresponding counterparts in general relativity (GR) through a phase transition triggered by tachyonic instability [16, 17], and stabilize due to nonlinear effects ultimately [18]. This process, called “spontaneous scalarization”, has been widely investigated in many generalized scalar-tensor theories [19–28]. In addition, the scalarized objects have garnered significant attention because the weak-field regions as the asymptotic part of their spacetimes do not violate current observations within the Solar System [29].

In the past decade, there has been growing interest in studying the structure of NSs within the framework of theories of gravity that include an additional vector field. A relatively simple theory with an extra vector field where the NS structure was obtained is the Einstein-æther theory [30, 31]. In this theory, a dynamical unit timelike vector field is coupled to gravity, thereby any solution of the vector field defines the 4-velocity of a local “preferred” frame at each spacetime point, breaking the local Lorentz symmetry. The maximal mass of a NS in the Einstein-æther theory is smaller compared to what is predicted by GR [32]. The discovery of a massive NS

would constrain parameters in the theory or even rule out this kind of vector æther field.

However, general vector-tensor theories do not require a fixed magnitude for the vector field. For example, there are two simplest nonminimal couplings,

$$\eta A^\mu A_\mu R, \quad \zeta A^\mu A^\nu R_{\mu\nu}, \quad (1)$$

where  $A^\mu$  is a vector field, in the Lagrangian of Hellings-Nordtvedt (HN) theory [33]. The static spherical NS solutions for the first type of coupling were calculated by Annulli *et al.* [34], and vectorized NS solutions were found within a certain range of  $\eta$ . However, such vectorized spherical stars must arise out of nonlinear effects (such as selected initial conditions) rather than from a linear mechanism originating from spherical GR stars. Additionally, some studies (see e.g. Refs. [35, 36]) pointed out that many theories of gravity involving nonminimally coupled vector fields face a challenge where triggers of spontaneous vectorization through tachyonic instability may also lead to ghost instability. Gradient instabilities, similar to the ghost instability, have also been found in black hole (BH) solutions in the bumblebee theory recently [37].

The Standard Model Extension (SME) is an effective field theory that describes various Lorentz symmetry breaking effects [38–40]. The bumblebee model can be treated as a concrete example of the minimal gravitational SME, and its action is [40, 41]

$$S = \int d^4x \sqrt{-g} \left( \frac{R}{2\kappa} + \frac{\xi}{2\kappa} B^\mu B^\nu R_{\mu\nu} - \frac{1}{4} B^{\mu\nu} B_{\mu\nu} - V(\cdot) \right) + S_m, \quad (2)$$

where  $g$  is the determinant of the metric  $g_{\mu\nu}$ , the constant  $\kappa \equiv 8\pi G$  with  $G$  being the gravitational constant, and  $S_m$  represents the action for matter fields. Here,  $B_\mu$  is the bumblebee field, and the field strength tensor is  $B_{\mu\nu} = \partial_\mu B_\nu - \partial_\nu B_\mu$ , similar to the electromagnetic field.

Unlike the HN theory, the bumblebee theory features a self-interaction potential,

$$V = V(B^\lambda B_\lambda \mp b^2). \quad (3)$$

\* Corresponding author: [lshao@pku.edu.cn](mailto:lshao@pku.edu.cn)

For a stable vacuum of spacetime, we require that the potential  $V$  is minimized at  $B_\mu = b_\mu$  and  $b^\mu b_\mu = \pm b^2$ . Thus, the Lorentz symmetry is *spontaneously* violated as the bumblebee field has a nonzero vacuum value  $\langle B_\mu \rangle = b_\mu$  with preferred spacetime directions.

There are two disparate approaches to solve the structure of astrophysical objects in the bumblebee theory of gravity in literature. One is to treat  $b^2$  as a parameter in Eq. (3) and solve for the dynamic field  $B_\mu$ , where  $b^2$  is usually set to be a constant to create a background with uniform magnitude [40, 41]. Páramos and Guiomar [42] considered this scenario with a harmonic oscillator potential

$$V = \frac{k}{2}(B^\lambda B_\lambda \mp b^2)^2, \quad k \neq 0, \quad (4)$$

where the time component of the vector field is set to zero ( $B_t = 0$ ) for simplicity. Another more common consideration suggests that the potential  $V$  is supposed to be minimized at the vacuum expectation value of the bumblebee field  $b_\mu$ . One then has

$$\left. \frac{dV}{d(B^\lambda B_\lambda)} \right|_{B_\mu=b_\mu} = 0. \quad (5)$$

The solution for astrophysical objects is based on the bumblebee field  $B_\mu$  being frozen in its vacuum expectation value. Therefore, the particular form of the potential driving its dynamics is irrelevant. Different assumptions about the vacuum expectation configuration result in various forms of the function  $b_\mu$ , which in turn lead to the emergence of different astrophysical structures. Typically, the constant-magnitude [43, 44] and divergence-free [45] conditions are applied.

In this work, we adopt the latter approach to solve for the static spherical NS solutions within the bumblebee theory. However, we do not impose any assumptions on the vacuum expectation value. There are two reasons for this approach. First, the assumption regarding the vacuum expectation value is not unique and lacks sufficient discussion about its validity. Second, under a specific assumption, the  $b_\mu$  typically does not satisfy the equations of motion for the vector field, as given in Eq. (7). This indicates that the vacuum solution does not stem from the spontaneous breaking of Lorentz symmetry at a certain energy scale.

One way to address this issue is to assume that the bumblebee field is coupled to the matter field, i.e. the Lagrangian of the matter field in Eq. (2) becomes a functional of the bumblebee field as well. This coupling introduces an additional vector flux from the matter field, which provides the necessary degrees of freedom to satisfy the equations of motion for the bumblebee field. Despite this, there are still some minor issues to be taken care of. It remains an open question whether there is any coupling between the bumblebee field and the matter sector outside the star. Additionally, the reasonableness of the assumption regarding the vacuum expectation value of

the bumblebee field when matter is present inside the star is also uncertain. Therefore, instead of imposing an artificial assumption on  $b_\mu$ , we treat the vacuum background as a specific solution of the theory resulting from the spontaneous breaking of Lorentz symmetry. In this case,  $b_\mu$  simply satisfies the equation of motion for  $B_\mu$  in the absence of coupling between the bumblebee field and the matter, provided that condition (5) is satisfied. In this scenario, a series of studies on bumblebee BH solutions have recently been conducted [37, 46–50].

For readers who are not familiar with the bumblebee theory, we strongly suggest viewing it simply as solving astrophysical objects in a vector-tensor theory, where the nonminimal coupling is given by the second type of Eq. (1). This is because, in the field equations, the potential and its first derivative terms are both zero for the background solution, and the equation of  $b_\mu$  is indistinguishable from the equation of  $A_\mu$ . The only difference is that  $A_\mu$  is a general vector field, while  $b_\mu$  is a background vector field that characterizes the breaking of Lorentz symmetry. We notice that the equivalence no longer holds when perturbations are made to the bumblebee field. Hence, our results are complementary to Annulli *et al.* [34], in which the authors solved the NS structure in the HN theory with the other coupling in Eq. (1), i.e.  $\eta A^\mu A_\mu R$ .

The paper is organized as follows. We start with setting up the equations and classification of solutions in Sec. II A, and a preliminary analysis of solutions is shown in Sec. II B. Section III introduces the numerical method that we apply to solve field equations, and discusses the parameter space for physical NS solutions. The numerical results for all possible coupling constant  $\xi$  are displayed in Sec. IV. Finally, we summarize our findings and give a brief outlook for the directions worthy of further study in Sec. V. The appendices list equations and figures to supplement the main text.

We use  $(-, +, +, +)$  as the sign convention for the metric and assume  $c = 1$  throughout the paper. We also apply the unit such that  $\kappa = 8\pi G = 1$  to avoid the repeated appearance in Sec. III, as well as in Appendices C and D. For quantities commonly encountered in astrophysics, we express them in more easily understandable units.

## II. EQUATIONS FOR STATIC SPHERICAL SOLUTIONS

The action (2) for the bumblebee gravity model yields the field equations for the tensor field and the vector field [40, 41, 46]

$$\mathcal{E}_{\mu\nu} \equiv G_{\mu\nu} - \kappa(T_{\mu\nu}^m + T_{\mu\nu}^{\text{vec}} + T_{\mu\nu}^\xi) = 0, \quad (6)$$

$$\mathcal{E}^\mu \equiv \nabla_\nu B^{\mu\nu} - \frac{\xi}{\kappa} R^{\mu\nu} B_\nu + 2B^\mu \frac{dV}{d(B^\lambda B_\lambda)} = 0, \quad (7)$$

where  $T_{\mu\nu}^m$  is the energy-momentum tensor for conventional matter, while the contributions from the massive

vector field and from nonminimal coupling between gravity and the bumblebee field are

$$T_{\mu\nu}^{\text{vec}} = g^{\alpha\beta} B_{\mu\alpha} B_{\nu\beta} - g_{\mu\nu} \left( \frac{1}{4} B^{\alpha\beta} B_{\alpha\beta} + V \right) + 2B_\mu B_\nu \frac{dV}{d(B^\lambda B_\lambda)}, \quad (8)$$

$$T_{\mu\nu}^\xi = \frac{\xi}{2\kappa} \left[ g_{\mu\nu} (R_{\alpha\beta} - \nabla_\alpha \nabla_\beta) B^\alpha B^\beta + 2\nabla_\alpha \nabla_{(\mu} (B_{\nu)} B^\alpha) - 4B^\alpha B_{(\mu} R_{\nu)\alpha} - \square (B_\mu B_\nu) \right]. \quad (9)$$

### A. Two classes of solutions

For static and spherical solutions, we use the metric ansatz

$$ds^2 = -e^{2\nu} dt^2 + e^{2\mu} dr^2 + r^2 (d\theta^2 + \sin^2 \theta d\phi^2), \quad (10)$$

where  $\mu$  and  $\nu$  are functions of the radial coordinate  $r$ . Further, we assume vanishing polar and azimuthal components of the bumblebee field, written as  $b_\mu = (b_t, b_r, 0, 0)$ . From now on, the bumblebee fields refer to those vacuum background configurations denoted as  $b_\mu$ . Then, the field strength tensor, defined as  $b_{\mu\nu} = \partial_\mu b_\nu - \partial_\nu b_\mu$ , takes the form

$$b_{\mu\nu} = \begin{pmatrix} 0 & -b'_t & 0 & 0 \\ b'_t & 0 & 0 & 0 \\ 0 & 0 & 0 & 0 \\ 0 & 0 & 0 & 0 \end{pmatrix}.$$

Here we assume that both  $b_t$  and  $b_r$  have only  $r$  dependence, and the prime denotes the derivative with respect to  $r$ . The field equations, with the ansatz of metric and vector field substituted, can be found in Appendix A.

With the help of the partial derivative formula for covariant divergence and Eq. (5), the components of Eq. (7) may be written as

$$\mathcal{E}^{\bar{\mu}} = \frac{1}{\sqrt{-g}} \partial_r (\sqrt{-g} b^{\bar{\mu}r}) - \frac{\xi}{\kappa} R^{\bar{\mu}\bar{\nu}} b_{\bar{\nu}}, \quad (11)$$

where there is no summation for the index  $\bar{\mu} = t, r, \theta, \phi$ . It is easy to find that  $\mathcal{E}^\theta = \mathcal{E}^\phi = 0$  automatically, and  $\mathcal{E}^t = 0$  leads to a second-order ordinary differential equation of  $b_t$ . Due to the symmetry of  $b^{\mu\nu}$ , the component  $\bar{\mu} = r$  gives

$$\xi R^{rr} b_r = 0. \quad (12)$$

Equation (12) gives two classes of solutions

$$\text{Class I: } b_r = 0, \quad (13a)$$

$$\text{Class II: } R_{rr} = 0. \quad (13b)$$

In the work on static spherical BH solutions of the bumblebee gravity [46], Class I that restricts the vector field corresponds to a family of vacuum solutions with 4 parameters, while Class II that restricts the spacetime geometry corresponds to a family of vacuum solutions with 6 parameters. In this paper, we only consider NS solutions of Class I.

### B. Approximate behaviors of the NS solutions

We expand the quantities near the center of a NS as,

$$\rho(r) = \sum_{n=0}^{\infty} \rho_n r^n, \quad (14a)$$

$$p(r) = \sum_{n=0}^{\infty} p_n r^n, \quad (14b)$$

$$\nu(r) = \sum_{n=0}^{\infty} \nu_n r^n, \quad (14c)$$

$$m(r) = \sum_{n=0}^{\infty} m_n r^n, \quad (14d)$$

$$b_t(r) = \sum_{n=0}^{\infty} b_n r^n, \quad (14e)$$

where  $\rho$  and  $p$  refer to the mass density and pressure respectively, and  $m$  is related to  $\mu$  by

$$e^{2\mu(r)} = \left( 1 - \frac{2Gm(r)}{r} \right)^{-1}. \quad (15)$$

After comparing equations of motion order by order, we have the non-vanishing leading-order coefficients,

$$m_3 = \frac{4\pi}{3} \frac{3p_0 b_0^2 (2\kappa - \xi) \xi + 2e^{2\nu_0} \kappa \rho_0}{2e^{2\nu_0} \kappa + \xi(\xi - 2\kappa) b_0^2}, \quad (16a)$$

$$b_2 = \frac{\kappa}{6} \frac{e^{2\nu_0} (3p_0 + \rho_0)}{2e^{2\nu_0} \kappa + \xi(\xi - 2\kappa) b_0^2} \xi b_0, \quad (16b)$$

$$\nu_2 = \frac{\kappa^2}{6} \frac{e^{2\nu_0} (3p_0 + \rho_0)}{2e^{2\nu_0} \kappa + \xi(\xi - 2\kappa) b_0^2}, \quad (16c)$$

$$p_2 = -\frac{\kappa^2}{6} \frac{e^{2\nu_0} (3p_0 + \rho_0)(p_0 + \rho_0)}{2e^{2\nu_0} \kappa + \xi(\xi - 2\kappa) b_0^2}. \quad (16d)$$

All higher-order coefficients can be acquired from the central values  $\rho_0$ ,  $p_0$ ,  $\nu_0$  and  $b_0$ . If  $b_0 = 0$ , then  $b_t(r) = 0$  since coefficients  $b_n \propto b_0$  for all  $n > 0$ . The remaining Eqs. (16a), (16c), and (16d) become

$$m_3 = \frac{4\pi}{3} \rho_0, \quad \nu_2 = \frac{2\pi}{3} G(3p_0 + \rho_0), \\ p_2 = -\frac{2\pi}{3} G(p_0 + \rho_0)(3p_0 + \rho_0), \quad (17)$$

which give the same NS structure as in GR.

TABLE I. Summary of conditions that go back to NS and spacetime solutions in GR.

Condition	Coefficients	Vector field
$b_0 = 0, \forall \xi$	Eq. (17), $b_2 = 0$	Vanishing
$\xi = 0, b_0 \neq 0$	Eq. (17), $b_2 = 0$	Constant
$\xi = 2\kappa, b_0 \neq 0$	Eq. (17), Eq. (19)	Nontrivial

The bumblebee model of gravity recovers the Einstein-Maxwell theory if  $V(\cdot) = 0$  and  $\xi = 0$  are used. In this situation, the equation for the vector field has the solution

$$b_t(r) = b_0 + \int_0^r \frac{q_0}{r'^2} e^{\mu(r') + \nu(r')} dr', \quad (18)$$

inside the star, where  $q_0$  is an integral constant. Since the bumblebee field has no source if  $\xi = 0$ , the possible solutions of  $b'_t$  is either zero ( $q_0 = 0$ ) or it represents the electric field generated by a point charge at the origin ( $q_0 \neq 0$ ). The latter is excluded due to the convergence requirement at the center, i.e.  $b'_t(0) = b_1 = 0$ . Another particular value of the coupling is  $\xi = 2\kappa$ , in which case Eq. (17) is also satisfied with

$$b_2 = \frac{1}{6}(3p_0 + \rho_0)b_0. \quad (19)$$

In conclusion, the GR solution of spacetime is recovered if  $\xi = 0$  or  $\xi = 2\kappa$ , equipped with a constant or non-trivial vector field respectively. Table I summarizes all conditions that give rise to NS solutions in GR if  $b_r = 0$ .

The asymptotic expansion of variables at infinity can be written as

$$\nu(r) = \sum_{n=1}^{\infty} \frac{\nu_{-n}}{r^n}, \quad (20a)$$

$$m(r) = M + \sum_{n=1}^{\infty} \frac{m_{-n}}{r^n}, \quad (20b)$$

$$b_t(r) = X + \frac{2\sqrt{\pi}Q}{r} + \sum_{n=2}^{\infty} \frac{b_{-n}}{r^n}. \quad (20c)$$

Here, all the high-order coefficients in the summation only depend on the Arnowitt-Deser-Misner (ADM) mass  $M$ , the background vector field  $X$ , and the vector charge  $Q$ . The factor  $2\sqrt{\pi}$  has been chosen so that the Reissner-Nordström metric is recovered for the vacuum solution when  $\xi = 0$ . The specific recurrence relations are displayed in Appendix B.

Nevertheless, only two of the quantities in  $\{M, X, Q\}$  are independent, as all three depend on just two central variables (see Sec. III). This can be clearly illustrated by the  $\xi = 2\kappa$  example whose exterior solution is the Schwarzschild spacetime, thereby one has the relation  $GMX + \sqrt{\pi}Q = 0$ . We point out that all the BH solutions are stealth Schwarzschild type if  $\xi = 2\kappa$  [46], which

indicates that the Birkhoff theorem is applicable in this case (at least for the  $b_r = 0$  class), i.e. the exterior solution of a spherically symmetric star is indeed a part of a BH solution of the theory.

### III. FORMALISM AND PARAMETER SPACE

To solve the static spherical NSs in the bumblebee theory, we assume  $b_\mu = (b_t(r), 0, 0, 0)$  and treat stars as perfect fluid equipped with an equation of state (EOS),  $p = p(\rho)$ . Therefore, the energy-momentum tensor of a NS constituted by conventional matter is

$$T_{\mu\nu}^m = (\rho + p)u_\mu u_\nu + pg_{\mu\nu}, \quad (21)$$

where  $u_\mu = (e^{\nu(r)}, 0, 0, 0)$  is the 4-velocity of matter, while  $\rho(r)$  and  $p(r)$  are energy density and pressure in a local inertial reference frame comoving with matter.

The Bianchi identity, together with the equations of motion in Appendix A, gives the modified Tolman-Oppenheimer-Volkoff (TOV) equations

$$p' = -(p + \rho)\nu', \quad (22)$$

$$\mu' = -\frac{\mathcal{D}}{\mathcal{E}r}, \quad (23)$$

$$\nu'' = \frac{\mathcal{A}}{r^2} + (\mu' - \nu')\left(\nu' + \frac{1}{r}\right), \quad (24)$$

$$b_t'' = \left(\mu' + \nu' - \frac{2}{r}\right)b_t' + \xi\left(\nu'' + \nu'^2 - \mu'\nu' + \frac{2}{r}\nu'\right)b_t, \quad (25)$$

where the prime denotes the derivative with respect to  $r$ , and the four functions of  $r$  are

$$\mathcal{A} \equiv r^2 \left[ pe^{2\mu} + \frac{1}{2}b_t'^2 - \xi b_t \nu' (b_t' - b_t \nu') e^{-2\nu} \right], \quad (26a)$$

$$\mathcal{B} \equiv \xi b_t [(\xi - 2)b_t - 4(b_t' - b_t \nu')r] r \nu' + 2r \nu' e^{2\nu} - e^{2\mu+2\nu}(\rho + p)r^2 + \xi b_t'^2 r^2, \quad (26b)$$

$$\mathcal{C} \equiv 2e^{2\nu} + \xi(\xi - 2)b_t^2, \quad (26c)$$

$$\mathcal{D} \equiv \mathcal{B} + \xi(\xi - 2)b_t^2 \mathcal{A}. \quad (26d)$$

We start the integration of modified TOV equations at the center of the star with boundary conditions<sup>1</sup>

$$\begin{aligned} \nu(0) &= \nu_0, & p(0) &= p_c, & \mu(0) &= 0, \\ \nu'(0) &= 0, & b_t(0) &= b_0, & b_t'(0) &= 0, \end{aligned} \quad (27)$$

<sup>1</sup> All the necessary first derivatives vanish due to the constraints imposed by the equations of motion. An alternative form of modified TOV equations, which makes this more apparent, is provided in Appendix C. This differs from scalar-tensor theories, where the first derivatives are often artificially set to zero.

TABLE II. Requirements on  $b_0$  for a given  $\nu_0$ .

Condition	$\xi < 0$	$0 < \xi < 2\kappa$	$\xi > 2\kappa$
$m_3 > 0$	$b_0^2 < \frac{2\rho_0}{3p_0} \frac{e^{2\nu_0 \kappa}}{\xi(\xi-2\kappa)}$	$b_0^2 < \frac{2e^{2\nu_0 \kappa}}{\xi(2\kappa-\xi)}$	$b_0^2 < \frac{2\rho_0}{3p_0} \frac{e^{2\nu_0 \kappa}}{\xi(\xi-2\kappa)}$
$p_2 < 0$	any $b_0$	$b_0^2 < \frac{2e^{2\nu_0 \kappa}}{\xi(2\kappa-\xi)}$	any $b_0$
No divergence <sup>a</sup>	$b_0^2 < (b_0^{\max})^2$	$X^2 < \frac{2\kappa}{\xi(2\kappa-\xi)} \Leftrightarrow b_0^2 < (b_0^{\max})^2$	any $b_0$

<sup>a</sup>  $b_0^{\max}$  represents the maximum value  $b_0$  that can be attained. It certainly depends on  $\xi$  and  $\rho_c$ , but it is hard to express analytically. There is no limit on  $b_0$  of singularity if a compact star is considered, i.e. for NSs with  $R < 20$  km, in the range  $\xi > 2\kappa$ .

where  $p_c = p(\rho_c)$ . The integration terminates on the stellar surface  $r = R$  where the pressure equals to zero.

To handle the situation at infinity, we consider the coordinate transformation

$$x = \frac{r - R}{r + \beta R}, \quad (28)$$

which maps the radius of the star to  $x = 0$  and maps the infinity to  $x = 1$ . Here,  $\beta \geq 0$  is a free parameter which controls the asymptotic behaviors of variables that are treated as functions of  $x$ . The modified TOV equations outside the star as functions of  $x$  are shown in Appendix D. Fortunately,  $x = 1$  is not a singularity of the differential equations, thereby the integration outside a NS can be calculated.

The radial component of the metric and the time component of the vector field can be expressed at infinity as

$$g^{rr}(r) = 1 - \frac{m(r)}{4\pi r}, \quad (29)$$

$$b_t(r) = X + \frac{q(r)}{r}, \quad (30)$$

where  $m(r)$  is given in Eq. (20b) and

$$q(r) = 2\sqrt{\pi}Q + \sum_{n=2}^{\infty} \frac{b_{-n}}{r^{n-1}}. \quad (31)$$

Differentiating Eq. (29) and Eq. (30) with respect to  $x$ , one finds

$$\dot{m} = \frac{(1 + \beta x)(1 - x)\dot{m} - (1 + \beta)m}{4\pi(1 + \beta x)^2 R} e^{2\mu}, \quad (32)$$

$$\dot{b}_t = \frac{(1 + \beta x)(1 - x)\dot{q} - (1 + \beta)q}{(1 + \beta x)^2 R}, \quad (33)$$

where the overdot denotes the derivative with respect to  $x$ . The ADM mass and the vector charge are then acquired by considering Eq. (32) and Eq. (33) at  $x = 1$  respectively,

$$M = m|_{x=1} = 8\pi(1 + \beta)R\dot{m}|_{x=1}, \quad (34)$$

$$Q = \frac{q|_{x=1}}{2\sqrt{\pi}} = -\frac{1 + \beta}{2\sqrt{\pi}} R\dot{b}_t|_{x=1}, \quad (35)$$

where  $(\dot{m} + \dot{v})_{x=1} = 0$  is used. One can define the Schwarzschild radius  $R_S \equiv M/4\pi$ . The stellar radius becomes smaller than its Schwarzschild radius (see e.g. Ref. [51]) if

$$2(1 + \beta)\dot{v}|_{x=1} > 1. \quad (36)$$

The modified TOV equations only guarantee  $g_{rr} = 1$  at infinity, and one needs to choose the central values  $p_c$ ,  $\nu_0$ , and  $b_0$  carefully to ensure  $g_{tt} = -1$ . In other words, the requirement of asymptotic flatness makes only two out of these three boundary variables  $\{p_c, \nu_0, b_0\}$  independent. To satisfy this, let us consider a coordinate transformation

$$t \rightarrow e^{-\Delta\nu} t,$$

while  $r$ ,  $\theta$  and  $\phi$  remain the same. The time components of the metric  $g_{\mu\nu}$  and the vector field  $b_\mu$  change correspondingly,

$$g_{tt} \rightarrow e^{2\Delta\nu} g_{tt}, \quad b_t \rightarrow e^{\Delta\nu} b_t.$$

Therefore, the system of Eqs. (22–25) is invariant under the transformation

$$\nu \rightarrow \nu + \Delta\nu, \quad b_t \rightarrow e^{\Delta\nu} b_t \quad (37)$$

for an arbitrary  $\Delta\nu$ , and the asymptotic flatness is easily satisfied after setting  $\Delta\nu = -\nu_\infty$ . Consequently, the boundary conditions switch to

$$\nu_0 \rightarrow \nu_c = \nu_0 + \Delta\nu, \quad b_0 \rightarrow b_c = e^{\Delta\nu} b_0. \quad (38)$$

The radius, ADM mass and vector charge of the NS, as well as the background vector field at infinity, change correspondingly as

$$R \rightarrow R, \quad M \rightarrow M, \quad Q \rightarrow e^{\Delta\nu} Q, \quad X \rightarrow e^{\Delta\nu} X. \quad (39)$$

Generally, the vector field at infinity is determined by the background cosmic evolution in the bumblebee theory. It is natural to assume that all the NS spacetime share the same asymptotic vector field,  $\bar{b}_\mu = (\bar{b}_t, 0, 0, 0)$ . Once the central density  $\rho_c$  and the background vector field  $\bar{b}_t$  are chosen, the boundary condition  $(p_c, \nu_c, b_c)$  is determined, which leads to a unique asymptotically flat

solution of a NS in the bumblebee theory with a given coupling constant  $\xi$ .

A positive  $m_3$  and a negative  $p_2$  in Eq. (17), which are guaranteed by a series of energy conditions, lead to a gravitational mass that increases with radius (i.e.  $dm/dr > 0$ ) and a pressure that decreases with radius (i.e.  $dp/dr < 0$ ) in GR. As an analogy, we display the requirements of parameters in the bumblebee theory in Table II, which are obtained assuming  $m_3 > 0$  in Eq. (16a) and  $p_2 < 0$  in Eq. (16d). On the one hand,  $m_3$  could be negative for all  $\xi$  except 0 and  $2\kappa$ , which means a negative gravitational mass near the center. A range of negative gravitational masses indicates that the vector field, as a portion of the gravitational force, exerts repulsion force, which might relate to the instability of stars. On the other hand,  $p_2$  can be positive and leads to an increasing pressure along the radius when  $0 < \xi < 2\kappa$ , which is considered unphysical for a relativistic star. Divergences frequently arise during the process of solving the modified TOV equations, which also constrain the values of variables at the stellar center. These are summarized in the last row of Table II, with specific details on the divergences discussed in Sec. IV. At last, we require that the radius of the star does not exceed 20 km, as we are interested in compact stars.

#### IV. NUMERICAL RESULTS

To numerically calculate the NS spacetime, we choose the AP4 EOS as an example. There is no qualitative difference between different EOSs for NSs in the bumblebee gravity theory. Solutions are separated into three different parts by two special values, namely  $\xi = 0$  and  $\xi = 2\kappa$ , and each of those is discussed in this section. Without loss of generality, we set  $\nu_0 = 0$  and assume  $b_0 > 0$ , numerically calculating NS solutions with all possible  $\rho_c$  and  $b_0$ . Some relevant quantities of NSs are computed, including the baryonic mass  $M_b$ ,

$$M_b = m_b \int n_b \sqrt{-g} u^0 d^3x = \int \rho_b e^\mu d^3x, \quad (40)$$

and three dimensionless quantities, compactness  $C$ , fractional binding energy  $f_b$ , and charge-to-mass ratio  $\alpha$ , defined as [52],

$$C \equiv \frac{GM}{R}, \quad f_b \equiv \frac{M_b}{M} - 1, \quad \alpha \equiv \frac{Q}{\sqrt{\kappa}M}. \quad (41)$$

Results are given below and in Appendix E.

##### A. The $\xi < 0$ case

In Fig. 1, we present the contour plot of the time component of the bumblebee field at infinity for  $\xi = -\kappa$  as an illustrative case for a negative coupling constant. When the boundary condition  $b_0 = 0$  is imposed, the modified

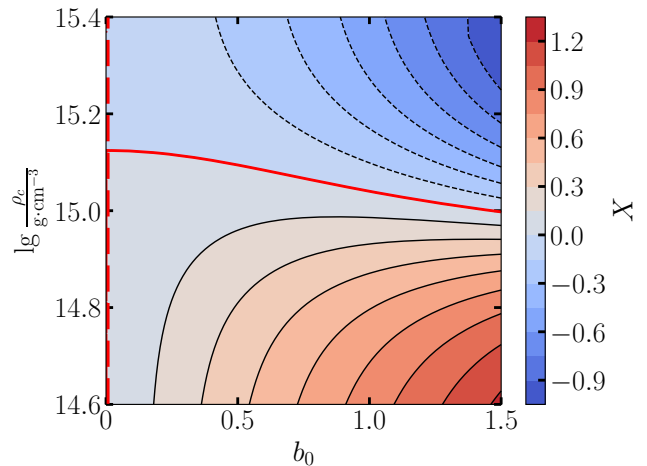


FIG. 1. Contour plot for the vector field at infinity [namely,  $X$  in Eq. (30)] on the  $b_0$ - $\rho_c$  plane for  $\xi = -\kappa$ . The black solid lines, red solid lines, and black dashed lines denote contours where  $X < 0$ ,  $X = 0$ , and  $X > 0$ , respectively. The vertical red dashed line corresponding to  $b_0 = 0$  represents the GR solutions, and the red solid curved line represents the vectorized solutions.

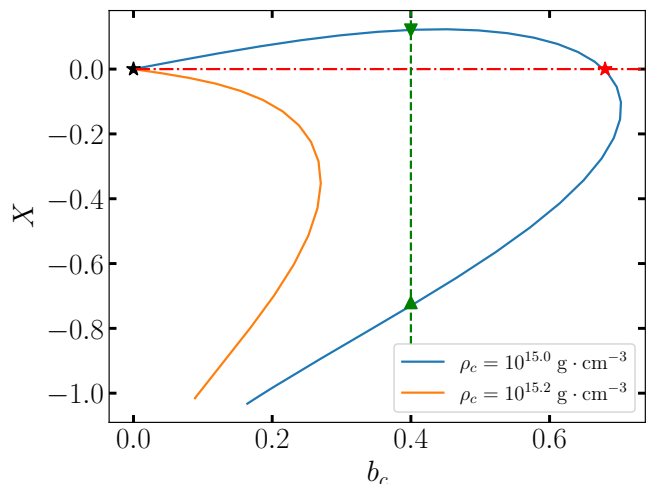


FIG. 2. The time component of vector field at infinity as a function of its central value of the star for  $\xi = -\kappa$ . The blue and orange curves represent two different central densities, and both of them terminate because of the divergence of  $g_{rr}$ . The black and red stars respectively denote a NS in GR and a vectorized NS, while the green triangle are NSs sharing the same vector field at stellar center.

TOV equations ensure that  $b_t(r) = 0$  throughout the spacetime, reducing the NS solutions to those found in GR, as indicated by the vertical red dashed line. The red solid curve represents solutions that exhibit the same asymptotic behavior as that in GR, including a cosmic background with  $\bar{b}_t = 0$ , but with a nontrivial vector field. These vectorized solutions are only found within a specific parameter space where  $\xi < 0$ .

In Fig. 2, we plot the relation between the vector fields at the center and at infinity. The blue and orange curves correspond to  $\rho_c = 10^{15.0} \text{ g} \cdot \text{cm}^{-3}$  and  $\rho_c = 10^{15.2} \text{ g} \cdot \text{cm}^{-3}$ , respectively. Any point on these curves which intersect the red dot-dashed line represents a vectorized NS, denoted by a red star, in contrast to a NS solution in GR, which is given by a black star. It is apparent that as the central density increases, the vectorized solution no longer exists. Therefore, there is an upper bound for  $\rho_c$  for vectorized solutions, which can be determined from the intersection of the two red lines in Fig. 1. While  $\rho_c$  does not theoretically have a lower bound, it cannot be too small given that we are considering compact stars and the radius should be less than 20 km.

Another interesting feature of the bumblebee theory is that it allows for two distinct asymptotically flat solutions with a same central density and vector field, as exemplified by the green triangles where  $\rho_c = 10^{15} \text{ g} \cdot \text{cm}^{-3}$  and  $b_c = 0.4$  in Fig. 2. The difference of boundary condition between these two solutions arises from the difference in the metric component  $g_{tt}$  at the center, more specifically from the difference in  $\Delta\nu$ , which is used to set the boundary conditions at infinity.

The mass-radius relation of NSs in the  $\xi = -\kappa$  bumblebee theory is shown in Fig. 3. The buff region, which is actually composed of numerous curves representing NSs with the same central density when viewed closely, marks the mass and radius of all possible NSs in this scenario. Each curve in the top (bottom) panel represents NSs that share the same vector field at the stellar center (at infinity). All dots correspond to specific stars, with different markers indicating different characteristics. If there is only one solution for a fixed central density  $\rho_c$  that satisfies the set of boundary conditions (a fixed  $b_c$  or  $X$ ), the corresponding NS is represented by a general point. However, if there are two solutions for a fixed  $\rho_c$ , such as the two green triangles in Fig. 2, they are labeled as triangular points. Clearly, an upward triangular point and a downward triangular point always appear in pairs, where the upward (downward) triangular point represents the NS with a larger (smaller) fractional binding energy  $f_b$ . The closest points on a curve form a pair of upward and downward triangular points, and additional pairs can be identified by removing known pairs and repeating the process. It is easy to imagine that there must be a point between the nearest pair of triangular points where the upward triangle and the downward triangle coincide, referring to the tangent points (the rightmost point for the same  $b_c$  case while the upmost point for the same  $X$  case) of the  $b_c$ - $X$  curve with the horizontal or vertical line in Fig. 2.

The black dashed line in Fig. 3 represents the mass-radius curve of a NS in GR. The black solid line, which represents vectorized NSs, bifurcates from this curve. We find that the vectorized NS has a larger binding energy compared to the NS in GR (explicitly illustrated in Fig. 7 in Appendix E) with the same central density, suggesting

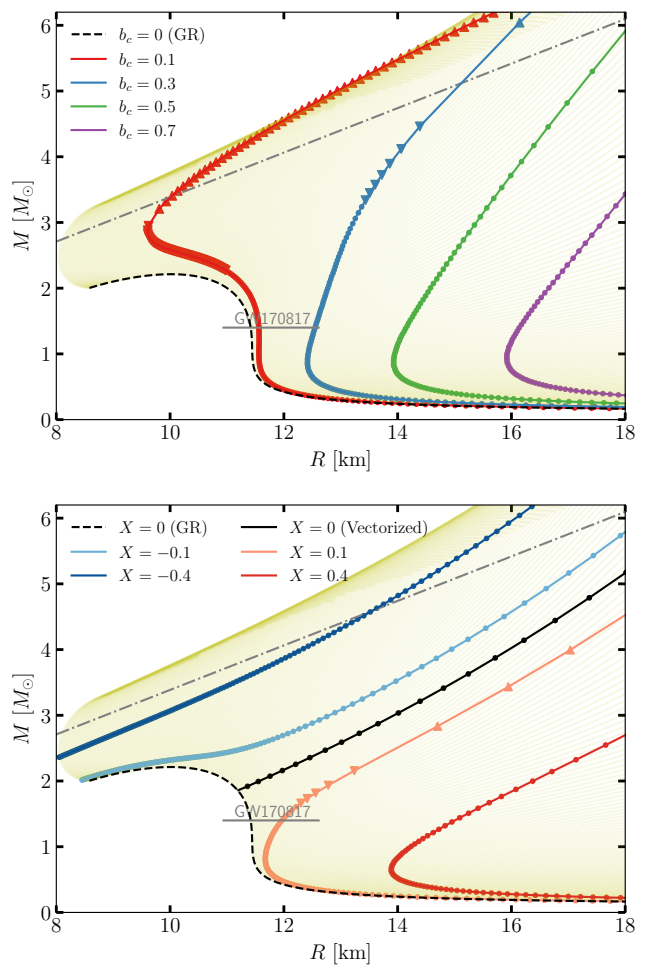


FIG. 3. The mass-radius curves of NSs for  $\xi = -\kappa$  with a same vector field at the center (top panel) and at infinity (bottom panel). The buff region represents all possible NSs in this case. In both panels, the black dashed line is the mass-radius curve of NSs in GR, the gray dot-dashed line denotes NSs with a compactness of 0.5, and the short gray bar marks the estimate of the radius of a  $M = 1.4M_\odot$  NS [53].

that vectorized stars are more energetically favorable. As the coupling becomes more negative, the corresponding bifurcation point has a lower central density, resulting in a shift toward the lower right of the mass-radius curve in GR. This result is quite similar to the findings by Annulli *et al.* [34] studying another form of nonminimal coupling  $\eta A^\mu A_\mu R$  in Eq. (1), which suggests a certain generality within vector-tensor theories.

The short gray bar indicates the estimate from GW170817 [12] for the radius of a  $M = 1.4M_\odot$  NS, with a 90% confidence level [53]. Given an EOS, the estimated value,  $R = 11.75^{+0.86}_{-0.81}$  km, can be used to constrain the vector field at infinity. Specifically, for the coupling  $\xi = -\kappa$ , the constraint is  $X \lesssim 0.17$ .

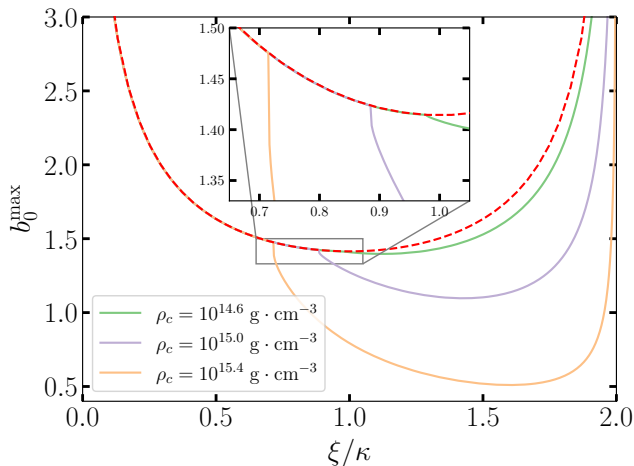


FIG. 4. The maximum value of  $b_0$  at different central densities when solving the modified TOV equations in the range  $0 < \xi < 2\kappa$ . The red dashed line represents  $p_2 = 0$  in Eq. (16d). Here we set  $\nu_0 = 0$ .

### B. The $0 < \xi < 2\kappa$ case

The parameter  $b_0$  also has an upper bound within the range  $0 < \xi < 2\kappa$ , as shown in Fig. 4 for three different central densities. Above the red dashed line, the pressure increases along the radial direction ( $p_2 > 0$ ), preventing being a star. However, the red line does not represent the strictest bound as the coupling becomes stronger, as indicated by the curves bifurcating from the red one. The reason for this lies in the asymptotic expansion equations of variables at infinity, discussed in Appendix B. For the expansion to be valid, the coefficients must remain finite, meaning that the denominator,  $2\kappa + \xi(\xi - 2\kappa)X^2$ , must be positive. This requirement imposes a smaller maximum  $b_0$  as  $\xi$  increases.

To compare these two distinct cases, we plot the mass-radius relation for both  $\xi = \kappa/2$  and  $\xi = \kappa$  in Fig. 5. For solutions where the maximum value of  $b_0$  is determined by  $p_2$ , the NS has a lower mass and a smaller radius, as shown in the top panel. However, when  $b_0^{\max}$  is constrained by the vector field at infinity, i.e. the right-hand side of the bifurcation point, the NS can become a lot more massive than those in GR. As  $b_0$  approaches its maximum value in this scenario,  $X$  simultaneously approaches the boundary where the denominator vanishes, leading to a dramatic increase in the ADM mass and vector charge of the NS. These extremely massive NSs have smaller radii compared to others, resulting in smaller baryonic masses and thus negative fractional binding energies. Although such extremely massive stars may not qualify as typical NSs due to their small radii, they remain significant as massive objects since they do not give rise to any singularities. They may constitute a new kind of exotic compact objects which are of central focus in the GW astrophysics studies [54]. Using the aforementioned

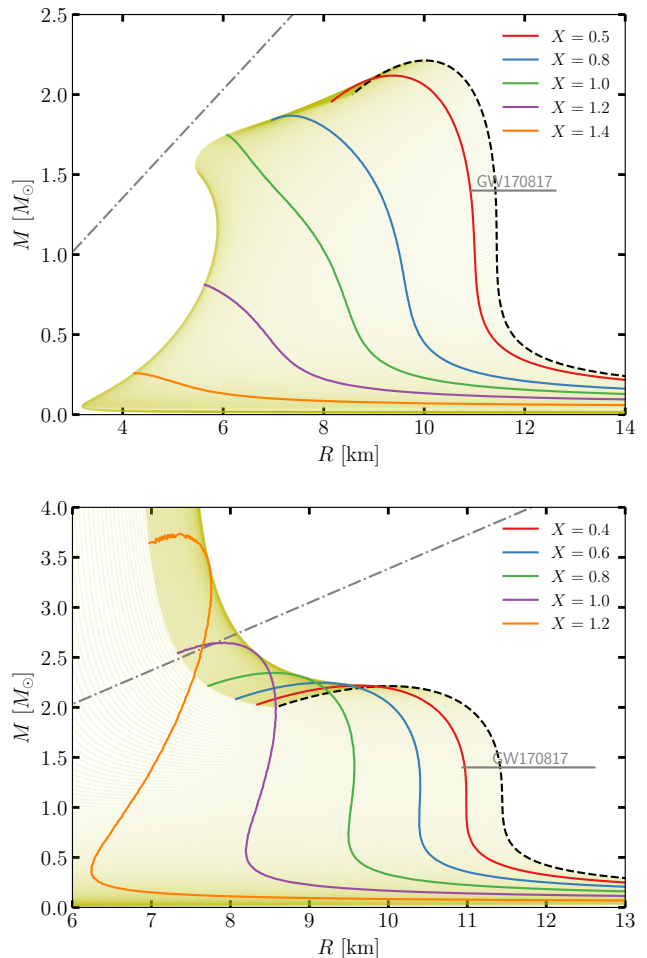


FIG. 5. The mass-radius curves of NSs for  $\xi = \kappa/2$  (top panel) and  $\xi = \kappa$  (bottom panel) in bumblebee theory with a same vector field at infinity. The buff region, the black dashed line, the gray dot-dashed line, and the short gray bar have the same meaning as in Fig. 3.

estimation of the NS radius, it is possible to constrain the range of the vector field at infinity, leading to  $X \lesssim 0.40$  for  $\xi = \kappa/2$  and  $X \lesssim 0.42$  for  $\xi = \kappa$ .

### C. The $\xi > 2\kappa$ case

The mass-radius relation in the remaining part of the parameter space is investigated for the representative case of  $\xi = 3\kappa$ , with the result shown in Fig. 6. It can be seen that in this parameter space, the radii of NSs in the bumblebee theory become larger. If using the previous estimation of radius from GW170817 [53] to impose constraints, we can conclude that the time component of the asymptotic vector field cannot exceed 0.62.

Comparing Fig. 3 and Fig. 6, it is found that the buff regions occupy similar positions in the mass-radius diagram, indicating some commonalities between parameter



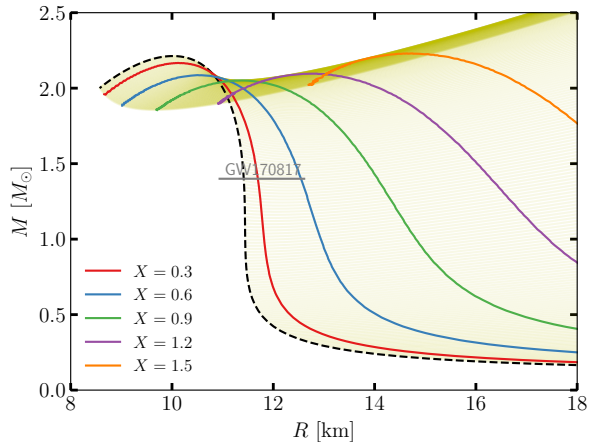


FIG. 6. The mass-radius curves of NSs for  $\xi = 3\kappa$  in bumblebee theory with a same vector field at infinity. The buff region, the black dashed line, and the short gray bar have the same meaning as in Fig. 3.

spaces  $\xi < 0$  and  $\xi > 2\kappa$ , as reflected by the same constraints on parameters shown in Table II. However, in the parameter space  $\xi > 2\kappa$ , NSs can move far along the positive direction of the radius and mass axes, and the corresponding solutions are free of singularities. This suggests that, in this case, extremely high-mass and large-radius stars are allowed, with positive fractional binding energy, unlike the massive stars in the parameter space  $0 < \xi < 2\kappa$ .

## V. SUMMARY

The bumblebee theory of gravity is an important vector-tensor theory with local Lorentz-symmetry violation. For the first time, we have numerically calculated the static spherical NS structure in this theory, exploring abundant characteristics of NSs under various different couplings.

For the two specific coupling parameters  $\xi = 0$  and  $\xi = 2\kappa$ , the solutions obtained here are consistent with those in GR. In the  $\xi = 0$  case, the solution permits a trivial vector field, while in the  $\xi = 2\kappa$  case, a non-trivial vector field is allowed while the exterior vacuum solution of the NS corresponds to a portion of the Schwarzschild solution. Using these two special couplings as boundaries, we divided the range of the coupling parameter  $\xi$  into three categories and discussed the characteristics of NS solutions for each of them.

Vectorized NS solutions appear when  $\xi < 0$ . These stars carry a nonzero vector charge and, as a result, can emit dipolar radiation when accelerated in binaries. The fractional binding energy of vectorized NSs is larger than the corresponding value of NSs in GR, indicating that the vectorized stars are energetically more favorable. We

also find that within this parameter range, two different NSs can have exactly the same central density and central vector field. The only difference between them is the spacetime geometry, even though both approach an asymptotically flat spacetime at infinity. For certain values of  $\xi$  within the range  $0 < \xi < 2\kappa$ , there are NS solutions with a large ADM mass but a small radius. In contrast, for  $\xi > 2\kappa$ , there are solutions where both the ADM mass and the radius of NSs are large. These solutions are mathematically self-consistent and may potentially be used to explain both observed and yet-to-be-detected special or exotic signals. Except for values of  $\xi$  slightly greater than 0, all other couplings result in scenarios where the stellar radius is smaller than the Schwarzschild radius corresponding to its ADM mass, i.e. the compactness  $C > 0.5$ . In addition to some theories of gravity that contain topological terms [51], NSs within the bumblebee theory can also exhibit this special property with extreme compactnesses.

Although the NS solutions in bumblebee theory exhibit a rich variety of behaviors, not all of these can satisfy observational constraints. We are the first to use the estimation from GW170817 of stellar radius of a  $M = 1.4M_\odot$  NS to constrain parameters. Different maximum values of the vector field at infinity were obtained for examples of different  $\xi$  discussed in Sec. IV. We also used the observed maximum mass of pulsars [55, 56] to constrain  $X$  as well, but this provides similar or less constraining limits, not to mention the large uncertainties from NS EOSs. Further constraints on the parameter space can be obtained by perturbing the obtained NS solutions, including calculating the tidal deformation and analyzing the stability of NSs, which could be the next stage of investigation. The effect of the self-interacting potential in Eq. (3) would emerge at the perturbation level, resulting in deviations from the HN theory that might reveal new aspects of Lorentz-symmetry violation.

In conclusion, as a generalization of the Einstein-Maxwell theory and an important example of Lorentz-violating gravity theories, the bumblebee model contains rich NS solutions. We here have provided the first set of comprehensive studies. Testing these solutions plays a significant role in fundamental physics. It might help us explore whether gravity is nonminimally coupled to a vector field similar to but beyond the electromagnetic field, and it could also aid in investigating whether a special local reference frame exists in the Universe.

## ACKNOWLEDGMENTS

We thank Zhanfeng Mai and Jinbo Yang for discussions. This work was supported by the National SKA Program of China (2020SKA0120300), the National Natural Science Foundation of China (11991053), the Beijing Natural Science Foundation (1242018), the China Postdoctoral Science Foundation (2023M741999), the Max Planck Partner Group Program funded by the Max

### Appendix A: Field Equations Using the Static Spherical Ansatz

Substituting ansatz (10) into the field equations, and assuming that the bumblebee 1-form field has only time component  $b_t$  and radial component  $b_r$ . The only two non-vanishing components of  $\mathcal{E}^\mu$  are

$$\mathcal{E}^t = - \left\{ b_t'' - \left( \mu' + \nu' - \frac{2}{r} \right) b_t' + \left[ \frac{\xi}{\kappa} \left( \mu' \nu' - \frac{2}{r} \nu' - \nu'' - \nu'^2 \right) - 2V_{\mathfrak{B}} e^{2\mu} \right] b_t \right\} e^{-2(\mu+\nu)}, \quad (\text{A1})$$

$$\mathcal{E}^r = \left[ \frac{\xi}{\kappa} \left( \mu' \nu' + \frac{2}{r} \mu' - \nu'' - \nu'^2 \right) - 2V_{\mathfrak{B}} e^{2\mu} \right] b_r e^{-4\mu}. \quad (\text{A2})$$

Here,  $V_{\mathfrak{B}} = dV/d\mathfrak{B} = dV/d(B^\lambda B_\lambda)$ , which is set to zero in the main text. The nonzero components of  $\mathcal{E}_{\mu\nu}$  are

$$\begin{aligned} \mathcal{E}_{tt} = & \frac{e^{2\mu} + 2r\mu' - 1}{r^2} e^{2\nu-2\mu} - \kappa(V_{\mathfrak{B}} + \rho) e^{2\nu} - \left( \frac{\kappa}{2} - \xi \right) b_t'^2 e^{-2\mu} \\ & + \xi \left\{ b_t'' - \left( \mu' + 4\nu' - \frac{2}{r} \right) b_t' + \left[ \left( 2\mu' \nu' - \frac{4}{r} \nu' - 2\nu'' + \nu'^2 \right) - \frac{2\kappa}{\xi} V_{\mathfrak{B}} e^{2\mu} \right] b_t \right\} b_t e^{-2\mu} \\ & - \xi \left\{ b_r'^2 + \left[ b_r'' - \left( 5\mu' - \frac{4}{r} \right) b_r' - \left( \mu'' - 3\mu'^2 - \frac{6}{r} \mu' + \frac{1}{r^2} \right) b_r \right] b_r \right\} \end{aligned} \quad (\text{A3})$$

$$\begin{aligned} \mathcal{E}_{rr} = & \frac{1 + 2r\nu' - e^{2\mu}}{r^2} + \kappa(V_{\mathfrak{B}} - p) e^{2\mu} + \left( \frac{\kappa}{2} b_t'^2 - \xi b_t b_t' \nu' + \xi b_t^2 \nu'^2 \right) e^{-2\nu} \\ & + \xi \left[ \left( \nu' + \frac{2}{r} \right) b_r' - \left( \nu'' + \nu'^2 - \frac{2}{r} \nu' - \frac{1}{r^2} \right) b_r \right] e^{-2\mu} - 2\kappa V_{\mathfrak{B}} b_r^2, \end{aligned} \quad (\text{A4})$$

$$\begin{aligned} \mathcal{E}_{\theta\theta} = & \left( \nu'' + \nu'^2 + \frac{\nu' - \mu'}{r} - \mu' \nu' \right) r^2 e^{-2\mu} + \kappa r^2 (V_{\mathfrak{B}} - p) - \left( \frac{\kappa}{2} b_t'^2 - \xi b_t b_t' \nu' + \xi b_t^2 \nu'^2 \right) r^2 e^{-2(\mu+\nu)} \\ & + \xi r^2 \left\{ b_r'^2 + \left[ b_r'' - \left( 5\mu' - 2\nu' - \frac{2}{r} \right) b_r' + \left( \nu'' - \mu'' + \nu'^2 - 3\mu' \nu' + 3\mu'^2 + \frac{\nu' - 3\mu'}{r} \right) b_r \right] b_r \right\} e^{-4\mu}, \end{aligned} \quad (\text{A5})$$

$$\mathcal{E}_{\phi\phi} = \sin^2 \theta \mathcal{E}_{\theta\theta}, \quad (\text{A6})$$

$$\mathcal{E}_{tr} = \mathcal{E}_{rt} = \kappa e^{2\mu} \mathcal{E}^r b_t = \kappa \mathcal{E}_r b_t. \quad (\text{A7})$$

### Appendix B: Asymptotic Expansions of Variables at Infinity

In fact, the equations of motion restrict  $g_{rr} = 1$  at infinity but leave the asymptotic value of  $g_{tt}$  free, which is denoted by  $\nu_\infty$ . Comparing equations of motion order by order gives the recurrence relations of coefficients in Eq. (20) as follows

$$\nu_{-1} = -GM, \quad (\text{B1})$$

$$m_{-1} = \frac{16\pi^2 \kappa (\kappa - 2\xi) \alpha^2 + 6\sqrt{\pi\kappa} \xi \alpha X + 3\kappa G \xi X^2 + \xi (\xi - 2\kappa) [8\pi^2 \kappa \alpha^2 + \frac{\xi}{2} (GX + \sqrt{\pi\kappa} \alpha) X] X^2 e^{-2\nu_\infty}}{2e^{2\nu_\infty} \kappa + \xi (\xi - 2\kappa) X^2} M^2, \quad (\text{B2})$$

$$\nu_{-2} = - \frac{2\pi\kappa^2 (\xi - \kappa) \alpha^2 + 2\sqrt{\pi\kappa} G \xi \alpha X + G^2 (2e^{2\nu_\infty} \kappa + \xi (\xi - \kappa) X^2)}{2e^{2\nu_\infty} \kappa + \xi (\xi - 2\kappa) X^2} M^2, \quad (\text{B3})$$

$$b_{-2} = - \frac{2\pi\kappa (\xi - \kappa) \alpha^2 + 2\sqrt{\pi\kappa} G \xi \alpha X + G^2 \xi X^2}{2e^{2\nu_\infty} \kappa + \xi (\xi - 2\kappa) X^2} \xi M^2 X, \quad (\text{B4})$$

$$\dots \quad (\text{B5})$$

Here,  $\alpha$  is the dimensionless charge-to-mass ratio defined as  $\alpha \equiv Q/\sqrt{8\pi GM}$ . The assumption of asymptotic flatness selects  $\nu_\infty = 0$ .

There are three free variables— $M$ ,  $X$ , and  $Q$ —that determine the vacuum solution. However, only two of these three variables are independent, both for BH solutions and NS solutions. For a spherically symmetric static BH in the

bumblebee theory,  $g_{tt}$  must be zero at the horizon where  $g^{rr}$  vanishes, leading to a constraint  $f^{\text{BH}}(\xi; M, Q, X) = 0$  [46]. In the case of a spherically symmetric, static NS, all variables are determined by the central density  $\rho_c$  and the central vector field  $b_c$  for a given EOS. Therefore, a similar constraint  $f^{\text{NS}}(\text{EOS}, \xi; M, Q, X) = 0$  must exist, indicating that the relation between the ADM mass, vector charge, and the background field depends on the coupling  $\xi$  as well as the specific EOS. If the expressions of  $f^{\text{BH}}$  and  $f^{\text{NS}}$ , as functions of  $M$ ,  $Q$  and  $X$ , are identical for any EOS of NSs and the same  $\xi$ , then we can conclude that an extended version of Birkhoff theorem holds in the bumblebee theory with this specific coupling.

Our numerical calculations reveal that, for any EOS and any boundary conditions at the center, the spacetime outside the NS is the Schwarzschild spacetime when  $\xi = 2\kappa$ . Previous numerical studies on BHs in this theory also found that all spherically symmetric, static BH solutions are stealth Schwarzschild, meaning that the spacetime is Schwarzschild with a nonzero  $b_t(r)$  when  $\xi = 2\kappa$ . This result supports the implication that an extended form of the Birkhoff theorem holds in this theory, at least for  $\xi = 2\kappa$ .

### Appendix C: Another Form of Modified TOV Equations

It is easy to notice that  $\mu$  and  $\mu'$  can be eliminated from the other variables by using the field equations. The expressions of  $\mu$  and  $\mu'$  are

$$\mu = \frac{1}{2} \ln \left[ \frac{\mathcal{F}r^2 + 2e^{2\nu}(1 + 2r\nu')}{2(1 + \mathbf{p})} \right] - \nu, \quad (\text{C1})$$

$$\mu' = \frac{2\nu' + 2[(1 + \mathbf{p})(\nu'' + \nu'^2)r - \mathbf{p}(1 + r\nu')r^{-1}] - e^{-2\nu}(1 + 2\mathbf{p})\mathcal{F}r}{2(1 + \mathbf{p})(1 + r\nu')}, \quad (\text{C2})$$

where  $\mathbf{p} = pr^2$ ,  $\varrho = \rho r^2$  and

$$\mathcal{F} = b_t'^2 - 2\xi b_t b_t' \nu' + 2\xi b_t^2 \nu'^2. \quad (\text{C3})$$

Then the equations of  $\nu$  and  $b_t$  become

$$\nu'' = \frac{\mathcal{V}}{\mathcal{N}}, \quad b_t'' = \frac{\mathcal{X}}{\mathcal{N}}, \quad (\text{C4})$$

where

$$\begin{aligned} \mathcal{V} = & e^{-2\nu}(2 - \xi)\xi b_t^2 \nu' \mathcal{F} r^2 (1 + 2\mathbf{p}) + 2e^{2\nu} \left\{ (1 + r\nu') [\varrho(1 + 2r\nu')r^{-1} - 4\nu'] + [3 + r\nu'(3 - 2r\nu')] \mathbf{p} r^{-1} \right\} \\ & + r b_t^2 \left\{ 2 + (\varrho - 2\xi)(1 + r\nu') + [5 + r\nu' - 2\xi(1 + r\nu')] \mathbf{p} \right\} + 2\xi b_t b_t' \nu' [2(1 + 2r\nu') - \varrho(1 + r\nu') - (1 - 3r\nu') \mathbf{p}] r \\ & + 2\xi b_t^2 \nu' \left\{ (2 + 3\mathbf{p})(2 - \xi) + r\nu' [2(1 - \xi - 2r\nu') + \varrho(1 + r\nu') + (9 - 4\xi - 3r\nu') \mathbf{p}] \right\}, \end{aligned} \quad (\text{C5})$$

$$\begin{aligned} \mathcal{X} = & e^{-2\nu}(2 - \xi)\xi b_t^2 b_t' \mathcal{F} r^2 (1 + 2\mathbf{p}) + 2e^{2\nu} \left\{ [\varrho b_t' + (\varrho + 3\mathbf{p})\xi b_t r^{-1}] (1 + 2r\nu') - [4 + (3 - 2r\nu') \mathbf{p}] b_t' \right\} \\ & + b_t'^3 r^2 [\varrho + \mathbf{p} - 2\xi(1 + \mathbf{p})] + 2\xi^2 b_t^3 r \nu'^2 (\varrho + \mathbf{p} - 2) + \xi b_t b_t'^2 r [2 + \varrho + 5\mathbf{p} - 2\xi(1 + \mathbf{p}) + 2(4 - \varrho + 3\mathbf{p})r\nu'] \\ & + 2\xi b_t^2 b_t' \left\{ (2 + 3\mathbf{p})(2 - \xi) + [\xi(2 - \varrho) + (\varrho - 4)r\nu' + (4 - 3\xi - 3r\nu') \mathbf{p}] r\nu' \right\}, \end{aligned} \quad (\text{C6})$$

$$\mathcal{N} = 2(1 + \mathbf{p})r\mathcal{C} = 2(1 + \mathbf{p})[2e^{2\nu} + \xi(\xi - 2)b_t^2]r. \quad (\text{C7})$$

The denominator  $\mathcal{N}$  linearly approaches zero when approaching the stellar center. To ensure that the equation is not singular at  $r = 0$ , the numerator must approach zero linearly or faster. A term-by-term analysis of  $\mathcal{V}$  and  $\mathcal{X}$  ultimately leads to the requirement that  $\nu' = b_t' = 0$  at  $r = 0$ .

### Appendix D: Differential Equations Outside a NS

Since  $\rho = p = 0$  outside the star, we only need to solve metric functions  $\nu$ ,  $\mu$  and the vector field  $b_t$ . The differential equations of  $\nu(x)$  and  $b_t(x)$  are

$$\ddot{\nu} = \frac{\mathcal{V}}{\mathcal{N}}, \quad \ddot{b}_t = \frac{\mathcal{X}}{\mathcal{N}}, \quad (\text{D1})$$

where the overdot represents the derivative with respect to  $x$ . With the following definitions,

$$\mathcal{F}(x) = \dot{b}_t^2 - 2\xi b_t \dot{b}_t \dot{\nu} + 2\xi b_t^2 \dot{\nu}^2, \quad (\text{D2})$$

$$\mathcal{C}(x) = 2e^{2\nu} + \xi(\xi - 2)b_t^2, \quad (\text{D3})$$

$$\mathcal{N}(x) = 2(1 + \beta)(1 + \beta x)\mathcal{C}(x), \quad (\text{D4})$$

$$\mathcal{H}(x) = (1 - x)(1 + \beta x)\dot{\nu}, \quad (\text{D5})$$

$\mathcal{V}$  and  $\mathcal{X}$  are given by

$$\begin{aligned} \mathcal{V} = & (1 + \beta x)\dot{b}_t^2 \left\{ 2(1 + \beta)(1 - \xi) - \xi[2e^{2\nu} + (\xi - 2)b_t^2]\mathcal{H}e^{-2\nu} \right\} - 8e^{2\nu}(1 + \beta)[\beta + (1 + \beta x)\dot{\nu}]\dot{\nu} \\ & + 2(1 + \beta x)\xi^2(2 - \xi)b_t^4 \dot{\nu}^2 \mathcal{H}e^{-2\nu} + 2(1 + \beta x)\xi b_t \dot{b}_t \dot{\nu} [2(1 + \beta) + (2 + \mathcal{C}e^{-2\nu})\mathcal{H}] \\ & - 4\xi b_t^2 \left\{ \beta(1 + \beta)(\xi - 2) + (1 + \beta x)[(1 + \beta)(\xi - 1) + 2\mathcal{H}]\dot{\nu} \right\} \dot{\nu}, \end{aligned} \quad (\text{D6})$$

$$\begin{aligned} \mathcal{X} = & -(1 + \beta x)\xi[2e^{2\nu} + (\xi - 2)b_t^2]\dot{\nu}^2 \mathcal{H}e^{-2\nu} - 4(1 + \beta)(1 + \beta x)^2 \xi^2 b_t^3 \dot{\nu}^2 \\ & + 2(1 + \beta x)\xi b_t \dot{b}_t^2 [(1 + \beta)(1 - \xi) + (2 + \mathcal{C}e^{-2\nu})\mathcal{H}] - 8e^{2\nu}\beta(1 + \beta)\dot{b}_t \\ & - 2\xi b_t^2 \left\{ 2\beta(1 + \beta)(\xi - 2) + (1 + \beta x)[(2 + \mathcal{C}e^{-2\nu})\mathcal{H} - 2(1 + \beta)\xi]\dot{\nu} \right\} \dot{b}_t. \end{aligned} \quad (\text{D7})$$

The expression of  $\mu$  and  $\dot{\mu}$  are then derived as

$$\mu = -\nu + \frac{1}{2} \ln \left[ \frac{1 + \beta + 2(1 - x)(1 + \beta x)\dot{\nu}}{1 + \beta} e^{2\nu} + \frac{(1 - x)^2(1 + \beta x)^2}{2(1 + \beta)^2} \mathcal{F} \right], \quad (\text{D8})$$

$$\dot{\mu} = -\dot{\nu} + \frac{(1 - x)(1 + \beta x)\xi}{2(1 + \beta)\mathcal{C}} [(\xi - 2)b_t^2 \mathcal{F} e^{-2\nu} - 2(\dot{b}_t - 2b_t \dot{\nu})^2]. \quad (\text{D9})$$

## Appendix E: Supplementary Results

Here we present three contour plots in Figs. 7–9 for the time component of the vector field at the center  $b_c$ , baryonic mass  $M_b$ , stellar radius  $R$ , time component of the vector field at infinity  $X$ , ADM mass  $M$ , vector charge  $Q$ , compactness  $C$ , fractional binding energy  $f_b$ , and charge-to-mass ratio  $\alpha$  on the  $b_0$ - $\rho_c$  plane. The three figures respectively depict the cases for  $\xi = -\kappa$ ,  $\xi = \kappa/2$ , and  $\xi = 3\kappa$ , with  $\nu_0 = 0$  taken for the solutions. The reason the case  $\xi = \kappa$  is not plotted is that, in this scenario, the mass and charge diverge in certain regions of the parameter space. We include these figures in this appendix as supplementary material to help readers look deeper into the NS solutions. Additionally, if future observations can place tight constraints on certain parameters, like the compactness or the charge-to-mass ratio, these figures could provide a helpful guidance.

- 
- |  |  |
|--|--|
| <p>[1] B. P. Abbott <i>et al.</i> (LIGO Scientific, Virgo), <i>Phys. Rev. Lett.</i> <b>123</b>, 011102 (2019), arXiv:1811.00364 [gr-qc].</p> <p>[2] M. Kramer <i>et al.</i>, <i>Phys. Rev. X</i> <b>11</b>, 041050 (2021), arXiv:2112.06795 [astro-ph.HE].</p> <p>[3] R. Abbott <i>et al.</i> (LIGO Scientific, VIRGO, KAGRA), (2021), arXiv:2112.06861 [gr-qc].</p> <p>[4] L. Shao and K. Yagi, <i>Sci. Bull.</i> <b>67</b>, 1946 (2022), arXiv:2209.03351 [gr-qc].</p> <p>[5] K. Akiyama <i>et al.</i> (Event Horizon Telescope), <i>Astrophys. J. Lett.</i> <b>930</b>, L17 (2022), arXiv:2311.09484 [astro-ph.HE].</p> <p>[6] L. Shao, <i>Lect. Notes Phys.</i> <b>1017</b>, 385 (2023), arXiv:2206.15187 [gr-qc].</p> <p>[7] Z. Hu, X. Miao, and L. Shao, in <i>Recent Progress on Gravity Tests: Challenges and Future Perspectives</i>, edited by</p> | <p>C. Bambi and A. Cárdenas-Avenidaño (2024) pp. 61–99, arXiv:2303.17185 [astro-ph.HE].</p> <p>[8] P. C. C. Freire and N. Wex, <i>Living Rev. Rel.</i> <b>27</b>, 5 (2024), arXiv:2407.16540 [gr-qc].</p> <p>[9] B. P. Abbott <i>et al.</i> (LIGO Scientific, Virgo), <i>Phys. Rev. X</i> <b>9</b>, 011001 (2019), arXiv:1805.11579 [gr-qc].</p> <p>[10] B. P. Abbott <i>et al.</i> (LIGO Scientific, Virgo), <i>Phys. Rev. Lett.</i> <b>121</b>, 161101 (2018), arXiv:1805.11581 [gr-qc].</p> <p>[11] B. P. Abbott <i>et al.</i> (LIGO Scientific, Virgo), <i>Phys. Rev. Lett.</i> <b>119</b>, 161101 (2017), arXiv:1710.05832 [gr-qc].</p> <p>[12] B. P. Abbott <i>et al.</i> (LIGO Scientific, Virgo, Fermi-GBM, INTEGRAL), <i>Astrophys. J. Lett.</i> <b>848</b>, L13 (2017), arXiv:1710.05834 [astro-ph.HE].</p> <p>[13] A. Goldstein <i>et al.</i>, <i>Astrophys. J. Lett.</i> <b>848</b>, L14 (2017),</p> |
|--|--|

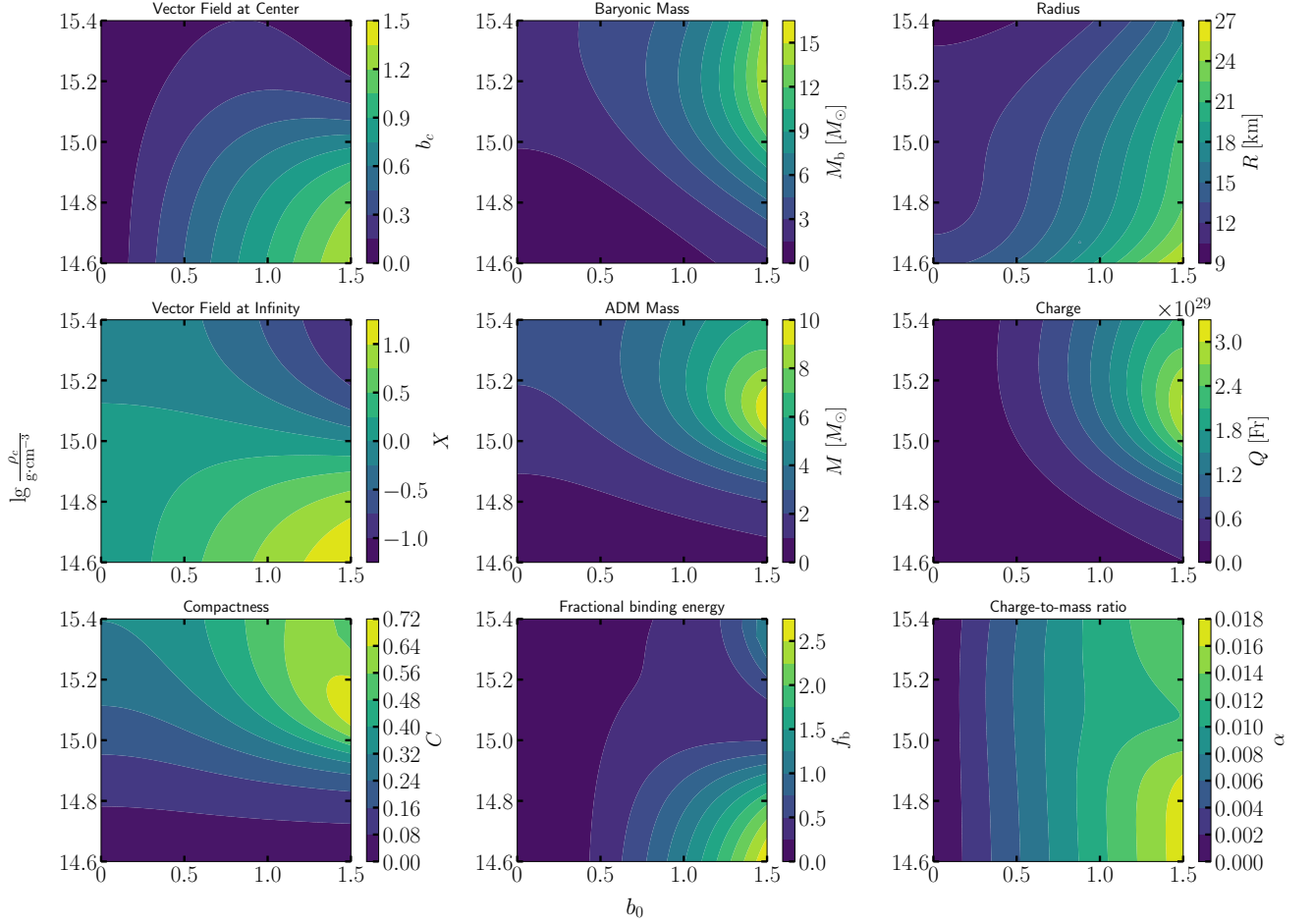


FIG. 7. Contour plots for nine quantities on the  $b_0$ - $\rho_c$  plane of NS solutions for a nonminimal coupling  $\xi = -\kappa$ : the vector field at center and infinity, baryonic and ADM masses, radius and charge of NSs, as well as the compactness, fractional binding energy, and charge-to-mass ration. The unit of the vector charge is Franklin ( $1 \text{ Fr} = 1 \text{ cm}^{3/2} \cdot \text{g}^{1/2} \cdot \text{s}^{-1}$ ) in Gaussian units. The largest  $b_0$  in horizontal axis does not reach its theoretical maximum  $b_0^{\text{max}}$ , and it is truncated at  $b_0 = 1.5$  to avoid stellar radii that are too large in the plot.

[arXiv:1710.05446 \[astro-ph.HE\]](#).

- [14] B. P. Abbott *et al.* (LIGO Scientific, Virgo, Fermi GBM, INTEGRAL, IceCube, AstroSat Cadmium Zinc Telluride Imager Team, IPN, Insight-Hxmt, ANTARES, Swift, AGILE Team, 1M2H Team, Dark Energy Camera GW-EM, DES, DLT40, GRAWITA, Fermi-LAT, ATCA, ASKAP, Las Cumbres Observatory Group, OzGrav, DWF (Deeper Wider Faster Program), AST3, CAAS-TRO, VINROUGE, MASTER, J-GEM, GROWTH, JAGWAR, CaltechNRAO, TTU-NRAO, NuSTAR, Pan-STARRS, MAXI Team, TZAC Consortium, KU, Nordic Optical Telescope, ePESSTO, GROND, Texas Tech University, SALT Group, TOROS, BOOTES, MWA, CALET, IKI-GW Follow-up, H.E.S.S., LOFAR, LWA, HAWC, Pierre Auger, ALMA, Euro VLBI Team, Pi of Sky, Chandra Team at McGill University, DFN, ATLAS Telescopes, High Time Resolution Universe Survey, RIMAS, RATIR, SKA South Africa/MeerKAT), *Astrophys. J. Lett.* **848**, L12 (2017), [arXiv:1710.05833 \[astro-ph.HE\]](#).
- [15] T. Damour and G. Esposito-Farèse, *Phys. Rev. Lett.* **70**, 2220 (1993).
- [16] T. Damour and G. Esposito-Farèse, *Phys. Rev. D* **54**, 1474 (1996), [arXiv:gr-qc/9602056](#).
- [17] N. Sennett, L. Shao, and J. Steinhoff, *Phys. Rev. D* **96**, 084019 (2017), [arXiv:1708.08285 \[gr-qc\]](#).
- [18] D. D. Doneva, F. M. Ramazanoğlu, H. O. Silva, T. P. Sotiriou, and S. S. Yazadjiev, *Rev. Mod. Phys.* **96**, 015004 (2024), [arXiv:2211.01766 \[gr-qc\]](#).
- [19] P. C. C. Freire, N. Wex, G. Esposito-Farèse, J. P. W. Verbiest, M. Bailes, B. A. Jacoby, M. Kramer, I. H. Stairs, J. Antoniadis, and G. H. Janssen, *Mon. Not. Roy. Astron. Soc.* **423**, 3328 (2012), [arXiv:1205.1450 \[astro-ph.GA\]](#).
- [20] S. S. Yazadjiev, D. D. Doneva, and D. Popchev, *Phys. Rev. D* **93**, 084038 (2016), [arXiv:1602.04766 \[gr-qc\]](#).
- [21] F. M. Ramazanoğlu and F. Pretorius, *Phys. Rev. D* **93**, 064005 (2016), [arXiv:1601.07475 \[gr-qc\]](#).
- [22] L. Shao, N. Sennett, A. Buonanno, M. Kramer, and N. Wex, *Phys. Rev. X* **7**, 041025 (2017), [arXiv:1704.07561](#)

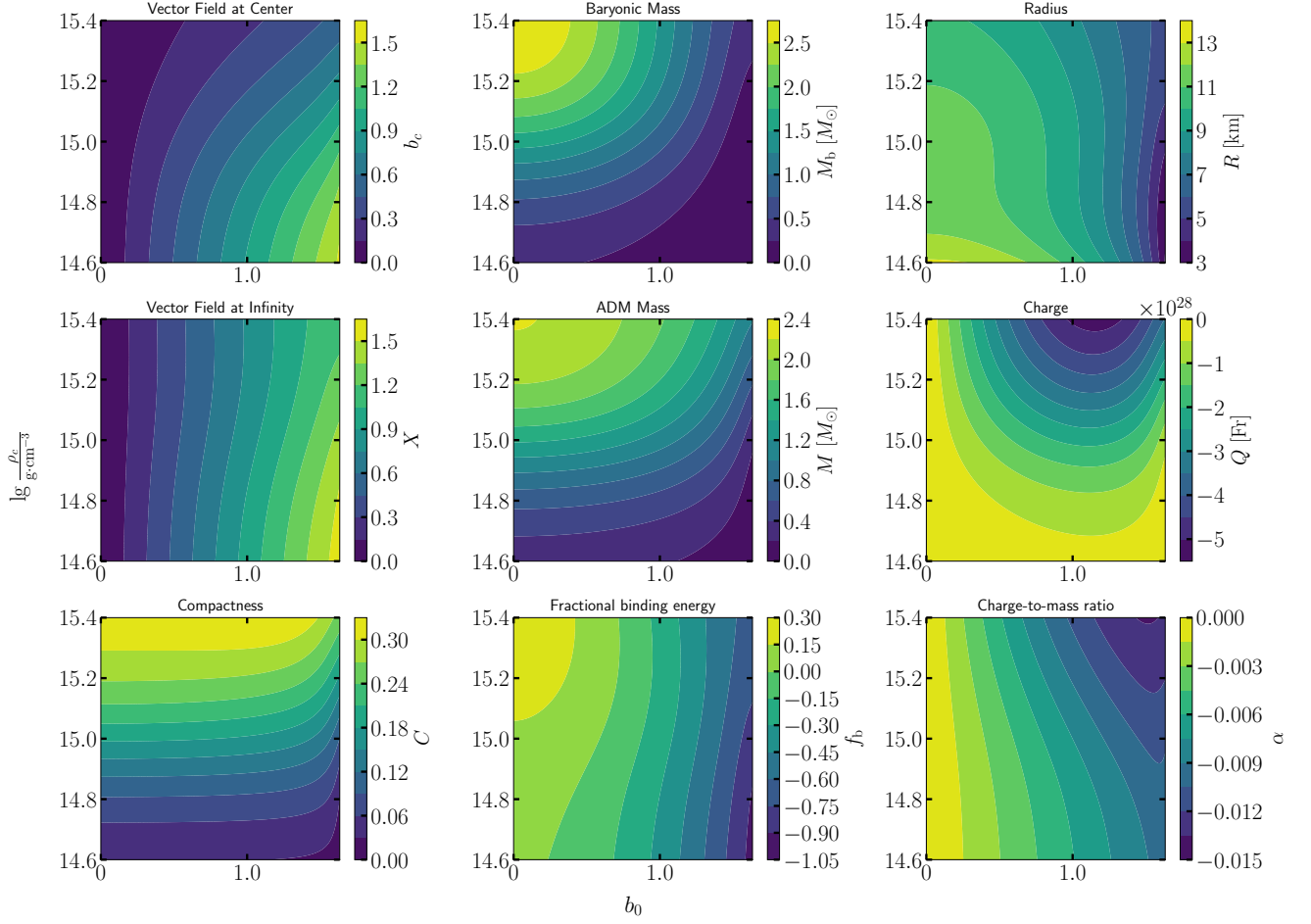


FIG. 8. Same as Fig. 7, but for  $\xi = \kappa/2$ . The largest value of the horizontal axis is  $\sqrt{2}$ , which is the maximum of  $b_0$  in this case.

- [gr-qc].
- [23] J. Zhao, P. C. C. Freire, M. Kramer, L. Shao, and N. Wex, *Class. Quant. Grav.* **39**, 11LT01 (2022), [arXiv:2201.03771 \[astro-ph.HE\]](#).
- [24] R. Xu, Y. Gao, and L. Shao, *Phys. Rev. D* **102**, 064057 (2020), [arXiv:2007.10080 \[gr-qc\]](#).
- [25] Z. Hu, Y. Gao, R. Xu, and L. Shao, *Phys. Rev. D* **104**, 104014 (2021), [arXiv:2109.13453 \[gr-qc\]](#).
- [26] H. O. Silva, J. Sakstein, L. Gualtieri, T. P. Sotiriou, and E. Berti, *Phys. Rev. Lett.* **120**, 131104 (2018), [arXiv:1711.02080 \[gr-qc\]](#).
- [27] D. D. Doneva and S. S. Yazadjiev, *Phys. Rev. Lett.* **120**, 131103 (2018), [arXiv:1711.01187 \[gr-qc\]](#).
- [28] R. Xu, Y. Gao, and L. Shao, *Phys. Rev. D* **105**, 024003 (2022), [arXiv:2111.06561 \[gr-qc\]](#).
- [29] C. M. Will, *Living Rev. Rel.* **17**, 4 (2014), [arXiv:1403.7377 \[gr-qc\]](#).
- [30] T. Jacobson, *PoS QG-PH*, 020 (2007), [arXiv:0801.1547 \[gr-qc\]](#).
- [31] K. Yagi, D. Blas, N. Yunes, and E. Barausse, *Phys. Rev. Lett.* **112**, 161101 (2014), [arXiv:1307.6219 \[gr-qc\]](#).
- [32] C. Eling, T. Jacobson, and M. Coleman Miller, *Phys. Rev. D* **76**, 042003 (2007), [Erratum: *Phys. Rev. D* **80**, 129906 (2009)], [arXiv:0705.1565 \[gr-qc\]](#).
- [33] R. W. Hellings and K. Nordtvedt, *Phys. Rev. D* **7**, 3593 (1973).
- [34] L. Annulli, V. Cardoso, and L. Gualtieri, *Phys. Rev. D* **99**, 044038 (2019), [arXiv:1901.02461 \[gr-qc\]](#).
- [35] H. O. Silva, A. Coates, F. M. Ramazanoğlu, and T. P. Sotiriou, *Phys. Rev. D* **105**, 024046 (2022), [arXiv:2110.04594 \[gr-qc\]](#).
- [36] E. S. Demirboğa, A. Coates, and F. M. Ramazanoğlu, *Phys. Rev. D* **105**, 024057 (2022), [arXiv:2112.04269 \[gr-qc\]](#).
- [37] Z.-F. Mai, R. Xu, D. Liang, and L. Shao, *Phys. Rev. D* **109**, 084076 (2024), [arXiv:2401.07757 \[gr-qc\]](#).
- [38] D. Colladay and V. A. Kostelecky, *Phys. Rev. D* **55**, 6760 (1997), [arXiv:hep-ph/9703464](#).
- [39] D. Colladay and V. A. Kostelecky, *Phys. Rev. D* **58**, 116002 (1998), [arXiv:hep-ph/9809521](#).
- [40] V. A. Kostelecky, *Phys. Rev. D* **69**, 105009 (2004), [arXiv:hep-th/0312310](#).
- [41] Q. G. Bailey and V. A. Kostelecky, *Phys. Rev. D* **74**, 045001 (2006), [arXiv:gr-qc/0603030](#).
- [42] J. Páramos and G. Guioamar, *Phys. Rev. D* **90**, 082002 (2014), [arXiv:1409.2022 \[astro-ph.SR\]](#).
- [43] R. Casana, A. Cavalcante, F. P. Poulis, and E. B. Santos, *Phys. Rev. D* **97**, 104001 (2018), [arXiv:1711.02273 \[gr-qc\]](#).

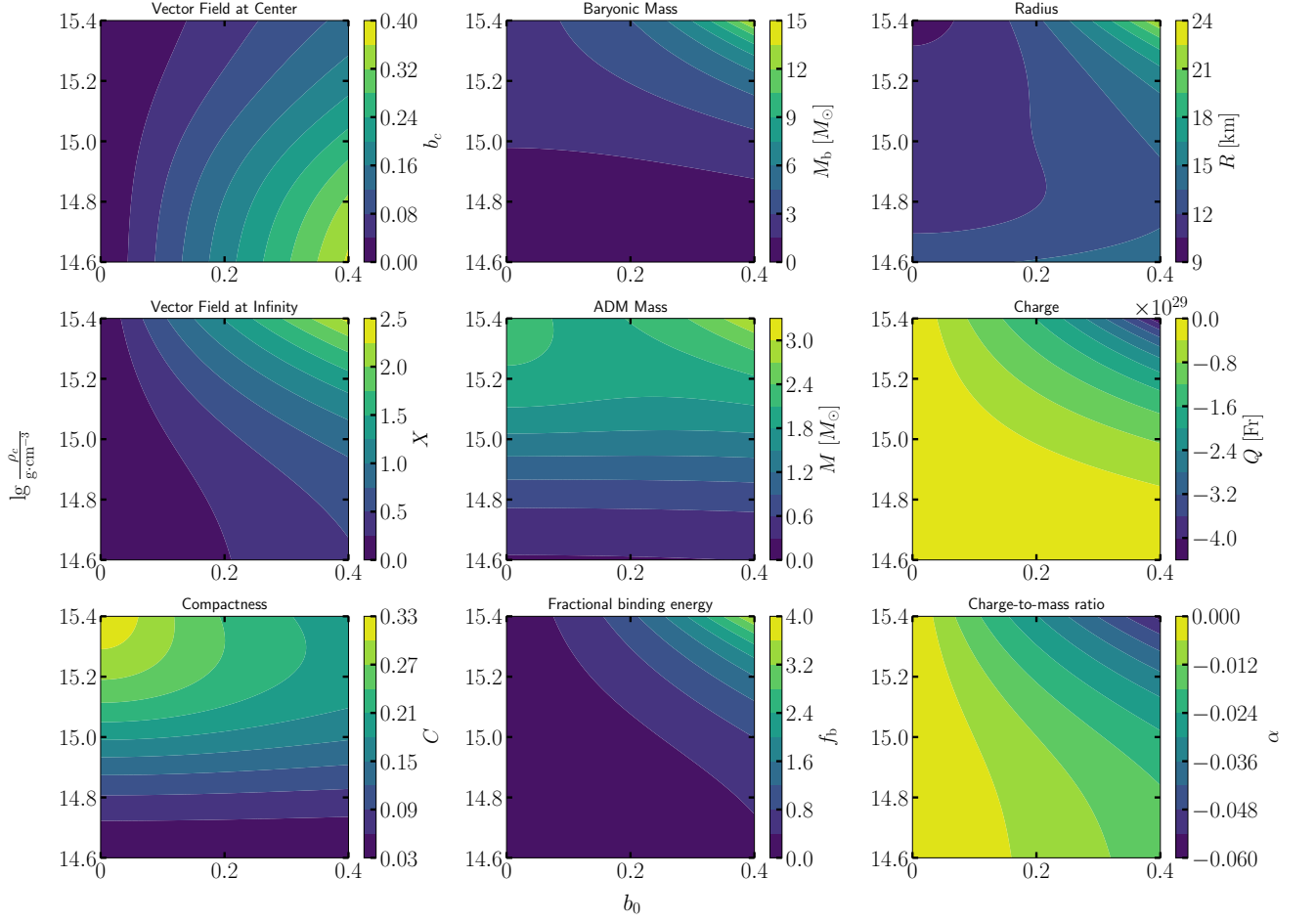


FIG. 9. Same as Fig. 7, but for  $\xi = 3\kappa$ . The horizontal axis is truncated at  $b_0 = 0.4$  to avoid stellar radii that are too large in the plot.

- qc].
- [44] J. C. S. Neves and F. G. Gardim, (2024), [arXiv:2409.20360 \[gr-qc\]](#).
- [45] O. Bertolami and J. Paramos, *Phys. Rev. D* **72**, 044001 (2005), [arXiv:hep-th/0504215](#).
- [46] R. Xu, D. Liang, and L. Shao, *Phys. Rev. D* **107**, 024011 (2023), [arXiv:2209.02209 \[gr-qc\]](#).
- [47] D. Liang, R. Xu, Z.-F. Mai, and L. Shao, *Phys. Rev. D* **107**, 044053 (2023), [arXiv:2212.09346 \[gr-qc\]](#).
- [48] R. Xu, D. Liang, and L. Shao, *Astrophys. J.* **945**, 148 (2023), [arXiv:2302.05671 \[gr-qc\]](#).
- [49] Z.-F. Mai, R. Xu, D. Liang, and L. Shao, *Phys. Rev. D* **108**, 024004 (2023), [arXiv:2304.08030 \[gr-qc\]](#).
- [50] Z. Hu, L. Shao, R. Xu, D. Liang, and Z.-F. Mai, *JCAP* **04**, 087 (2024), [arXiv:2312.02486 \[astro-ph.HE\]](#).
- [51] S. Li, H. Lü, Y. Gao, R. Xu, L. Shao, and H. Yu, (2023), [arXiv:2312.01406 \[gr-qc\]](#).
- [52] C. W. Misner, K. S. Thorne, and J. A. Wheeler, *Gravitation* (W. H. Freeman, San Francisco, 1973).
- [53] T. Dietrich, M. W. Coughlin, P. T. H. Pang, M. Bulla, J. Heinzel, L. Issa, I. Tews, and S. Antier, *Science* **370**, 1450 (2020), [arXiv:2002.11355 \[astro-ph.HE\]](#).
- [54] V. Cardoso and P. Pani, *Nature Astron.* **1**, 586 (2017), [arXiv:1709.01525 \[gr-qc\]](#).
- [55] E. Fonseca *et al.*, *Astrophys. J. Lett.* **915**, L12 (2021), [arXiv:2104.00880 \[astro-ph.HE\]](#).
- [56] J. Antoniadis *et al.*, *Science* **340**, 6131 (2013), [arXiv:1304.6875 \[astro-ph.HE\]](#).